BER the international journal of bridge engineering management and research

Numerical Simulation of a Long-Span Steel Truss Bridge Subjected to Blast Loads

Huihui Li[1,*]; Anil K. Agrawal[2]; Qian Chen[3]; and Hongfan Wang[2]

Submitted: 29 October 2024 **Accepted:** 16 December 2024 **Publication date:** 10 January 2025

DOI: 10.70465/ber.v2i1.17

Abstract: Few studies have focused on the blast load effects on steel truss bridges. To address this research gap, this article conducts an extensive investigation of the above-deck blast loads on a long-span steel truss bridge. The nonlinear dynamic response and damage modes of reinforced concrete (RC) deck and steel truss members of the bridge under different intensity levels of blast loads are numerically studied using the Load_Blast_Enhanced (LBE) function and Multi-Material Arbitrary Lagrangian-Eulerian (MM-ALE) method in LS-DYNA, to identify a cost-efficient approach with reasonable accuracy to simulate a long-span steel truss bridge subjected to blast loads. The LBE method has proved to be more conservative and cost-efficient than the MM-ALE method for simulating blast load effects on structures. A high-fidelity finite element model of the bridge (i.e., I-35W truss bridge) in LS-DYNA based on the multi-scale modeling technique and the LBE function to simulate blast loads is developed to investigate the structural response under several blast scenarios. The effectiveness of ultra-high-performance concrete (UHPC) in protecting the steel truss members from blast load effects has also been investigated. The results provide valuable insights for bridge owners on the probable response and possible protective measures for long-span steel truss bridges against intensive blast loads.

Author keywords: Steel truss bridges; blast loads; multi-scale modeling technique; above-deck denotations; UHPC strengthening

Introduction

There has been a global increase in blast attacks worldwide, particularly in recent decades.[1,2] Highway bridges are critical parts of the transportation network and the failure on a critical route may cause substantial economic loss and societal impacts, and more importantly, loss of life. Highway bridges are also considered attractive targets because of their accessibility and potential impacts on economic activities.[2–4] As one of the most famous collapse events, the collapse of the I-35W steel truss bridge has demonstrated the profound impact of long-span bridge collapses on the local economy and public psychology. Although investigations of blast load effects on buildings have been extensively performed over recent decades, studies on the structural response of highway bridges subjected to blast loads remain limited.[1] Additionally, current bridge design codes provide minimal guidelines for the protective design of highway bridges under intensive blast loads.[1] This emphasizes the need to incorporate extreme blast load considerations into the protective design of highway bridges.[2–5]

Approaches for analyzing the structural responses to blast loads generally fall into three different categories: (i) simplified analytical methods, (ii) numerical simulations, and (iii) experimental tests.[6] Most of the current structural design codes primarily utilize simplified analytical methods to estimate the structural response to prescribed blast loads.[6–8] Several commercial programs, such as AUTODYN,[9] ABAQUS,[10] and LS-DYNA,[11] are available for the numerical simulations of structures subjected to blast loads. These programs offer in-depth insights into the blast load effects on the structural response and damage modes of target structures.[1–3,12–15] Many previous studies have examined the failure modes of reinforced concrete (RC) structures subjected to blast loads, such as RC columns,[16,17] RC slabs,[18] and RC beams.[19] Typical failure behaviors of RC members resulting from blast loads can also be categorized by the scaled distance (Z).[6] Likewise, numerous studies have conducted both the experimental and numerical investigations of blast load effects on the steel members.[21–24]

However, few studies have investigated the protective design and the assessment of blast resistance of highway bridges through both field tests and numerical simulations. For instance, Hao and Tang[25] numerically investigated the damage propagation of a cable-stayed bridge under blast loads generated from a 1000 kg TNT explosion. They presented numerical simulations for several bridge components

*Corresponding Author: Huihui Li. Email: huihui.li@polyu.edu.hk
[1]Department of Civil & Environmental Engineering, The Hong Kong Polytechnic University, Hong Kong, 999077, China
[2]Department of Civil & Environmental Engineering, The City College of New York, New York, NY 10031, USA
[3]Thornton Tomasetti, New York, NY 10271, USA

Discussion period open till six months from the publication date. Please submit separate discussion for each individual paper. This paper is a part of the Vol. 1 of the International Journal of Bridge Engineering, Management and Research (© BER), ISSN 3065-0569.

to multiple blast loading levels. Williamson et al.[16,17] conducted blast tests and numerical simulations on RC columns to investigate the response and damage modes. Different damage levels in RC columns were observed under different blast intensity levels. Similarly, Williams and Williamson[26] found that the failure modes of RC columns could change from global minor cracks to brittle shear failure at the column base. Pan et al.[27] numerically investigated the blast load effects on an RC composite slab-on-girder bridge through the multi-Euler domain method. They investigated the dynamic performance and damage mechanisms of the whole bridge and identified the critical blast events. By taking a typical three-span simply supported RC bridge as a case study, Yi et al.[2,3] proposed a hybrid blast loading simulation approach by combining two common numerical methods for simulating blast loads in LS-DYNA, and they categorized various damage levels and failure behavior of different bridge components under blast loads. Pan et al.[28] presented extensive numerical analyses simulating the performance of three RC bridges under various detonation scenarios. They have examined both the localized damage mechanisms and global structural responses of these bridges. More recently, Zhu et al.[29] numerically investigated the failure mechanisms of several box girder bridges under-vehicle explosions. They found severe concrete spalling and fracture of steel bars when denotations occurred above the girder.

The aforementioned studies indicate that RC bridges or components could suffer severe damage under blast loads. Although it is impossible to shield highway bridges from blast attacks completely, rehabilitation techniques could substantially mitigate their effects.[1,25] Various retrofitting materials, such as Fiber reinforced polymer (FRP),[30] CFRP,[31] glass FRP,[32] and ultra-high-performance concrete (UHPC),[33–35] have been employed to enhance the blast loading resistance of structures,[6] in which UHPC strengthening of RC columns, RC beams, and RC slabs has been extensively investigated by many previous studies.[36,37] These studies suggest that UHPC strengthening is an effective retrofit measure to improve the load-carrying capacity of RC structures. Thus, this study proposes to use UHPC as a retrofit measure to retrofit the bridge deck of long-span truss bridges to enhance the blast resistance of the steel truss members under the targeted bridge decks (i.e., exposed to explosion attacks).

The above current state of the literature shows that relatively less attention has been focused towards the structural response and damage behavior of steel truss bridges under blast loads. In this research, comprehensive numerical simulations of various above-deck blast scenarios have been carried out for the I-35W steel truss bridge as a case study. The use of UHPC in limiting damages to the steel truss members caused by the above-deck explosions has also been investigated.

Finite Element Model of I-35W Steel Truss Bridge Subjected to Blast Loads

The I-35W steel truss bridge, with a main span of 140 m and two side spans of 81 m each, collapsed on August 1, 2007, killing 13 and injuring 145 people. The cause of this tragic failure was attributed to an under-designed gusset plate. This bridge has been widely used as a case study in several studies because of the detailed information available on its design and investigations.[38–47] As seen from several validation examples in Li[2] (i.e., steel cantilever beam, simply-supported steel truss, and steel truss bridge), the multi-scale modeling technique by using the Hughes-Liu beam with shell elements in LS-DYNA in simulating the nonlinear dynamic responses of structures to blast loads has been validated to be effective and reliable. Fig. 1 shows the schematic illustration of the numerical modeling of the cantilever beam in LS-DYNA using the shell elements only and the multi-scale modeling technique using the Hughes-Liu beam with shell elements, respectively.

As illustrated in Fig. 1b, the Hughes-Liu beam and shell elements were connected by a rigid body link with all degrees of freedom (DOFs) coupled. This approach has been used to develop a high-fidelity finite element (FE) model of the I-35W steel truss bridge, as shown in Fig. 2. This figure also shows two different blast cases at the center-span of the bridge. A blast zone has been designated for the blast in the middle of the center-span. For each of the blast cases in the blast zone, two-panel truss systems (each being 11.58 m long) were modeled using the multi-scale modeling

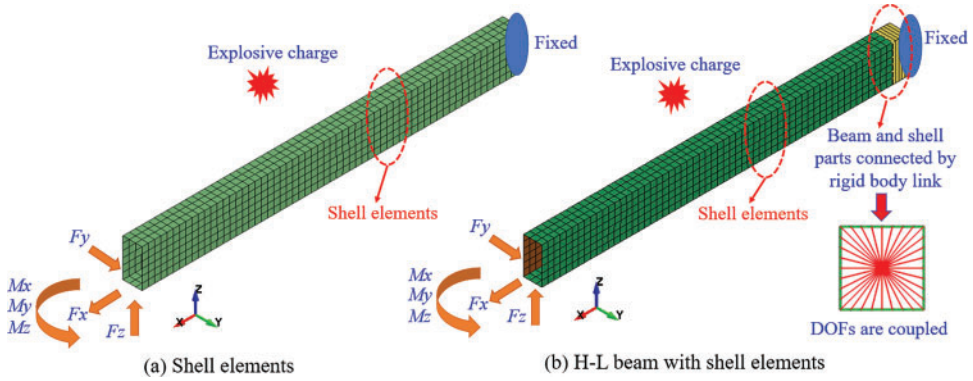

Figure 1. Schematic illustration of FE modeling of the cantilever beam: (a) shell elements and (b) Hughes-Liu beam with shell elements

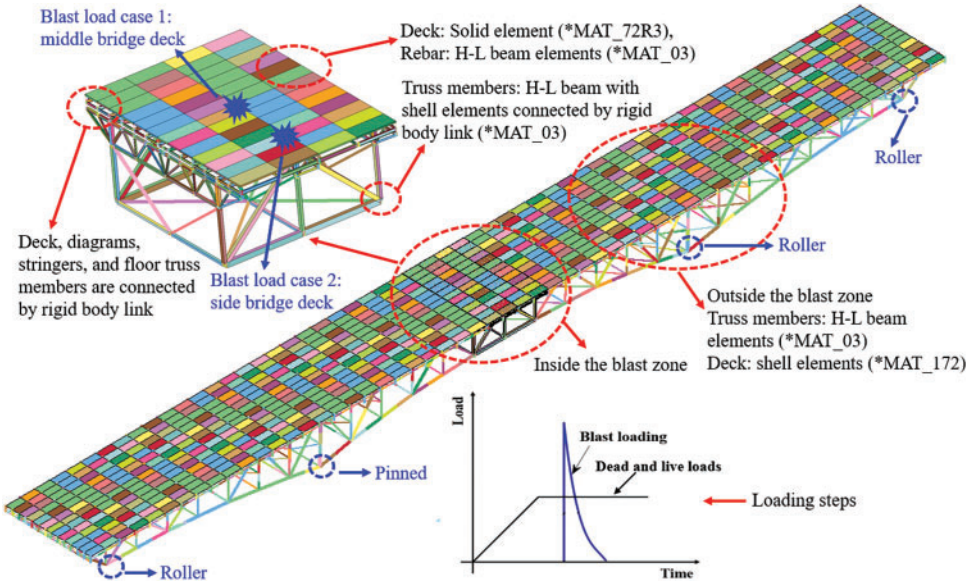

Figure 2. Numerical modeling of I-35W truss bridge under the above-deck explosions at the center-span

approach. Concrete_Damage_Rel3 (MAT_72R3) material model was used to simulate the behavior of the RC deck, and the strain rate effect of concrete was considered, whereas MAT_Plastic_Kinematic (MAT_03) was utilized to model the behavior of the steel truss members and reinforcements. The primary advantage of MAT_72R3 is its default parameter generation function, which is based on the unconfined compressive strength of the concrete. Detailed information on these material models can be found in the LS-DYNA user manual.[11] Table 1 shows the input parameters for the used material models. The strain rate effect of steel (i.e., truss members and steel bars) was considered using the Cowper and Symonds model.[20,21,24,35] The blast pressure segment set was defined on the top surface of the deck through the Load_Blast_Segment_Set formulation in LS-DYNA. For each blast location case, a mesh size of 20 mm for the deck and truss members inside the blast zone was used, whilst that for the deck outside the blast zone was 100 mm.

The truss members outside the blast zone were modeled using the Hughes-Liu beam formulation. An initial imperfection of $\Delta = L/100$ (L is the length of the truss member) was considered for each truss member to investigate the buckling behavior.[2,44,45] Material models MAT_Concrete_EC2 (MAT_172) and MAT_03 in LS-DYNA were used to simulate the RC deck (with the shell elements) and steel truss members (using the Hughes-Liu beam formulation), respectively. The Constrained_Lagrange_In_Solid formulation in LS-DYNA was applied to model the concrete deck-rebar interaction, and perfect bonding was assumed. In addition, rigid body links were employed for the nodal groups shared by the deck, stringers, and floor truss systems. The erosion technique was applied by using the MAT_Add_Erosion function. Simulation results showed that using a principal strain of 0.15 could provide reliable predictions of RC deck responses of the bridge.

Table 1. Material parameters of the concrete and steel members of the bridge

Material	Material model	Parameter	Value
Concrete	MAT_72R3	ρ_c (Density)	2403 kg/m^3
		ν_c (Poisson's ratio)	0.2
		f_c (Uniaxial compression strength)	28.0 MPa
		RSIZE	39.72
		UCF	1.45×10^{-4}
Steel	MAT_03	ρ_s (Density)	8901 kg/m^3
		E (Young's modulus)	200 GPa
		ν_s (Poisson's ratio)	0.3
		f_y (Yield stress)	345 MPa
		E_t (Tangent modulus)	1.068 GPa
		ε (Failure strain)	0.15

In addition, the Rayleigh damping model was used during the numerical analyses. During the transient analysis in LS-DYNA, the global damping could be defined using the system damping constant, D_s, in the keyword Damping_Global in LS-DYNA, which could be calculated as the critical damping factor, $(D_s)_{\text{critical}}$, corresponding to the fundamental frequency of the structure[11] and could be represented by Eq. (1) below, where the natural frequency $\omega_{\min}$ (in radians per unit time) can be taken as the fundamental frequency of the structure. A 2% critical damping was used during the simulations in this study. It should be noted that before the numerical simulations on the blast load effect on the truss bridges, the eigenvalue analysis (i.e., similar to the modal analysis) should be performed to verify the dynamic characteristics of the bridge. Details regarding the validation of the developed LS-DYNA model of the I-35 truss bridge could be referred to Li.[2]

$$(D_s)_{\text{critical}} = 2\omega_{\min} \tag{1}$$

The major components of the I-35W steel truss bridge include the RC deck and steel truss members. In all the expected blast load scenarios, the blast would occur at a certain distance (e.g., 1 m) above the concrete deck, and blast load effects would be propagated to the steel truss members after the deck was damaged. Blast loads could be applied on the deck using the Multi-Material Arbitrary Lagrangian-Eulerian (MM-ALE) method, which involves modeling the air around the bridge deck, and the Load_Blast_Enhanced (LBE) function in LS-DYNA (which does not require modeling of air). Generally, the MM-ALE method is suitable for multi-material interaction problems involving fluids and structures, but its application to long-span bridges may require substantial computational resources because of the large model size. In contrast, the LBE method is comparatively simpler and more computationally feasible. Thus, in the following subsections, we have conducted a comparison of these two methods to predict the blast response of RC decks based on the available test results in the literature, aiming to identify the most practical, simpler, and computationally efficient method for long-span steel truss bridges.

Verification of Blast Load Effects on the Concrete Deck

Based on the available test results in Wang et al.,[48] numerical simulations of RC decks under various blast load levels were conducted by using the LBE and MM-ALE methods in LS-DYNA. Blast loads were generated by the denotation of 0.2 to 0.46 kg TNT at a height of 0.4 m above the deck, as shown in Fig. 3. The concrete had a cylinder compressive strength of 39.5 MPa, a tensile strength of 4.2 MPa, and elastic modulus of 28.3 GPa. The steel reinforcements had a yield strength of 600 MPa, elastic modulus of 200 GPa, and Poisson's ratio of 0.3, respectively.

Material Models and Strain Rate Effects

Air can be simulated by using the MAT_Null formulation with a linear polynomial equation of state (EOS) in LS-DYNA, and it could be generally assumed as an ideal gas. Similarly, high explosives could be simulated by using the MAT_High_Explosive_Burn formulation with the Jones-Wilkens-Lee (JWL) equation of state in LS-DYNA. We used the default parameters for these material models. Material model MAT_72R3 was used to simulate the concrete. When RC structures are subjected to blast loads, concrete and steel may experience high strain rates, ranging from 10 to 1000 s^{-1} or even higher. At these strain rates, the strength of these materials could increase by over 100% for concrete under compression and by over 600% and 50% for concrete and reinforcing steel under tension, respectively.[49] Thus, the strain rate effects on concrete and steel should be considered for reliable simulations of structural response under blast loads. The influence of higher loading rates on concrete strength can be considered through a dynamic increase factor (*DIF*), also known as the ratio of dynamic-to-static strength versus strain rate, within the material model MAT_72R3 in LS-DYNA. *DIF* for concrete compressive strength (*CDIF*) and *DIF* for tensile strength (*TDIF*) can be

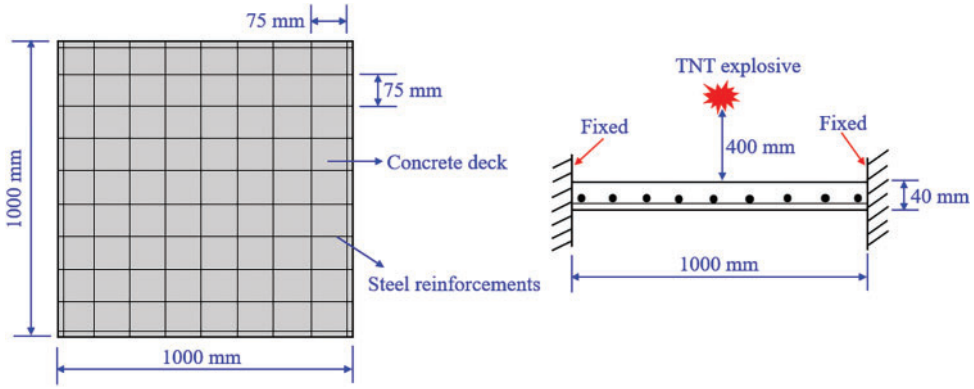

Figure 3. Geometry of RC deck

defined by Eqs. (2) and (3) below, respectively.[49,50]

$$CDIF = \frac{f_{cd}}{f_{cs}} = \begin{cases} \left(\frac{\varepsilon_{cd}}{\varepsilon_{cs}}\right)^{1.026\alpha} & \text{for} \quad \varepsilon_{cd} \le 30\ \text{s}^{-1} \\ \gamma \left(\frac{\varepsilon_{cd}}{\varepsilon_{cs}}\right)^{1/3} & \text{for} \quad \varepsilon_{cd} > 30\ \text{s}^{-1} \end{cases} \tag{2}$$

where ε_{cd} is the strain rate in the range of 30×10^{-6} to 300 s^{-1}; ε_{cs} is the strain rate (30×10^{-6} s^{-1}); f_{cd} is the dynamic compressive strength at ε_{cd}; f_{cs} is the dynamic compressive strength at ε_{cs}; $\alpha = (5 + 9\, f_{cs}/f_{co})^{-1}$; $\log \gamma = 6.15\alpha - 0.492$; and f_{co} equals 10 MPa.

$$TDIF = \frac{f_{td}}{f_{ts}} = \begin{cases} \left(\frac{\varepsilon_{td}}{\varepsilon_{ts}}\right)^{\delta} & \text{for} \quad \varepsilon_{td} \le 1\text{s}^{-1} \\ \beta \left(\frac{\varepsilon_{td}}{\varepsilon_{ts}}\right)^{1/3} & \text{for} \quad \varepsilon_{td} > 1\text{s}^{-1} \end{cases} \tag{3}$$

where ε_{td} is the strain rate in the range of 10^{-6} to 160 s^{-1}; ε_{ts} is the strain rate (10^{-6} s^{-1}); f_{td} is the dynamic compressive strength at ε_{td}; f_{ts} is the dynamic compressive strength at ε_{ts}; $\delta = (1 + 8\ f_{cs}/f_{co})^{-1}$; and $\log\ \beta = 6\delta - 2$. We used these default values of parameters in the material model MAT_72R3 in LS-DYNA to consider the strain rate effect of concrete. In addition, the steel reinforcements within the concrete deck were simulated by using the material model MAT_03 in LS-DYNA, which is a strain-sensitive uniaxial elastic–plastic material model that considers the strain rate sensitivity and stress-strain history dependence of steel.[11] In this material model, the high strain rate effect is considered using the Cowper and Symonds model, which scales the yield stress with the factor *DIF* as:

$$DIF = 1 + \left(\frac{\varepsilon^*}{C}\right)^{\frac{1}{P}} \tag{4}$$

where ε^* is the material strain rate. The C and P constant coefficients can be set equal to 40.4 and 5.0, respectively, as suggested in several previous studies for mild steel.[20,21,24,35] To simulate the physical fracture, shear failure, cratering, spalling, and crushing of concrete under blast loads, the erosion algorithm is usually employed. The erosion technique can be achieved by using the MAT_Add_Erosion function in LS-DYNA. After intensive simulations, it was found that using the principal strain of 0.15 as the erosion criterion of concrete could lead to reliable predictions of structural responses of RC decks.

Blast Load Simulation by Using the LBE Method

In modeling the bridge deck, the 8-node constant stress solid elements were used to simulate the concrete, whereas the steel reinforcements were modeled by using the Hughes-Liu beam formulation in LS-DYNA. To capture the localized damage modes of RC decks with high fidelity, the mesh size used for the concrete and steel bars was 5 mm, the Constrained_Lagrange_In_Solid formulation in LS-DYNA was

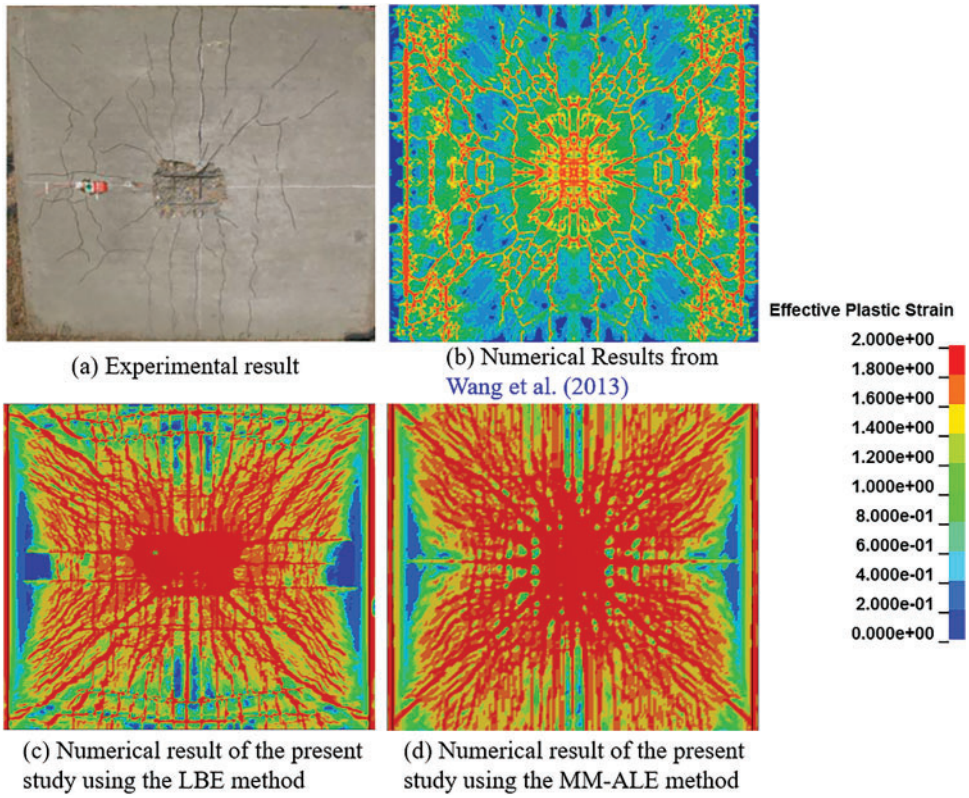

Figure 4. Comparison of the experimental and numerical damage modes for RC deck S2 using the LBE and MM-ALE methods (0.31 kg TNT)

used for modeling the concrete-rebar interaction, and perfect bonding was assumed. This mesh size was determined by performing the mesh convergence analysis. It was found that the use of the smaller elements (2.5 mm) for the concrete and reinforcing bars gave similar simulations but significantly increased the computational time. The Hourglass control formulation in LS-DYNA was used during the numerical simulations to prevent zero-energy modes.

Figs. 4 and 5 show the damage modes of RC decks based on both the experimental and numerical results by using the LBE and MM-ALE methods, respectively. It should be mentioned that the damage level of concrete could be identified by the effective plastic strain in the material model MAT_72R3, which is a scaled damage measurement parameter. The effective plastic strain ranges from 0 to 2, where 0 indicates no damage (elastic), 2 indicates complete failure (elastic–plastic), and a value between 1 and 2 represents concrete softening.[49] As observed from Fig. 4, due to the low tensile strength of concrete, a tensile spalling on the bottom surface of the deck was observed. Additionally, the calculated damaged area on the bottom side from the numerical simulation from Wang et al.[48] and that from the present study are shown in Figs. 4b and 4c, respectively. The radius of the damaged area was approximately 90 mm from the experimental test by Wang et al.[48]. This value was 100 mm in this study and that from Wang et al.,[48] which was slightly larger than the experimental one but represented a reasonable and conservative prediction, given the complexity of modeling blast load effects on structures. Similarly, as seen in Fig. 5, the radius of the damaged area of the deck obtained from the experimental test by Wang et al.[48] was approximately 120 mm, while that from the numerical simulation in this study was about 140 mm. Thus, the aforementioned observations indicate that the crack distribution and area of concrete crushing obtained from both the numerical simulations in this study and those by Wang et al.[48] agreed well with the experimental ones. These results demonstrate that the LBE function could yield acceptable simulation results of blast load effects on a bridge deck.

Blast Load Simulation by Using the MM-ALE Method

In this part, the MM-ALE method was utilized to perform the numerical simulations of the deck under different blast loads. Due to the presence of detonation products, the Donor Cell with Half-Index-Shift advection algorithm (METH = 3) in the keyword Control_ALE in LS-DYNA was used. The spherical shape of the explosive was simulated by using the keyword Initial_Volume_Fraction_Geometry, and the non-reflecting boundary conditions were imposed on the six surfaces of the modeled air medium by using the keyword Boundary_Non_Reflecting in LS-DYNA. In addition, the keyword Control_MPP_Decomposition_Distribute_ALE_Elements in LS-DYNA was utilized to achieve a good parallel processing performance. The numerical results were compared with the experimental ones available in the literature. Similar to the numerical results of RC decks using the

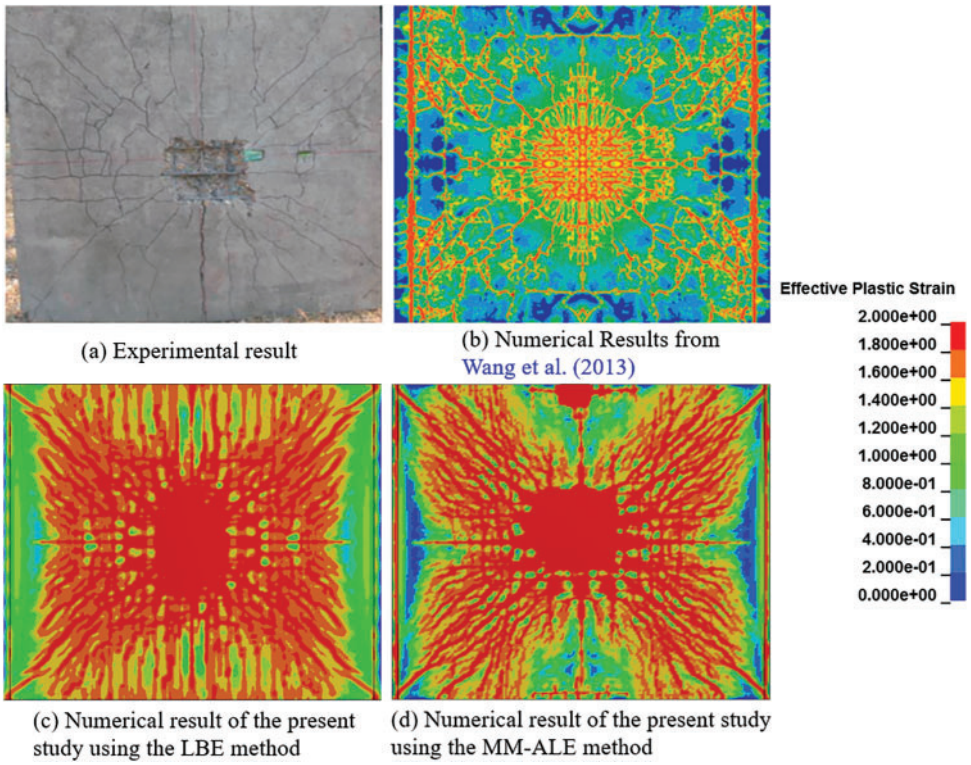

Figure 5. Comparison of the experimental and numerical damage modes for RC deck S3 using the LBE and MM-ALE methods (0.46 kg TNT)

LBE method, Figs. 5c and 5d show the damage modes of RC decks developed by using the MM-ALE method. It is observed that the simulation results were in good accordance with the experimental ones, and the damage modes (crack distributions and area of concrete crushing) by the MM-ALE method were relatively closer to the test results than the LBE method. However, the LBE method has notable advantages over the MM-ALE method in terms of computational time and memory requirement, as presented in Table 2. These factors are critical when simulating blast load effects on a long-span steel truss bridge.

Further comparisons between the LBE and MM-ALE methods were conducted using an example of the RC column. Details of modeling and simulation for this case can be found in Li.[2] Table 2 shows a comparison of the numerical results obtained from the LBE and MM-ALE methods in simulating the structural response of RC columns under blast loads. As discussed in Li,[2] the experimentally obtained peak pressure and maximum displacement of the column were 7.5 MPa and 12.5 mm, respectively. As seen from Table 2, the relative errors between the experimental peak pressures and the numerical ones obtained by using the LBE and MM-ALE methods were 8% and 4%, respectively. Similarly, these relative errors were 11.2% and 3.2%, respectively, for the maximum displacement. These results show that a relatively better accuracy can be achieved by using the MM-ALE method than the LBE approach in simulating the blast load effects on concrete structures. Besides, Table 2 also shows the comparison between the two methods in terms of the computational time and number of elements. It is observed that the LBE method had a significantly lower computational cost, with a computational time of 3.5 hours compared to 33.5 hours for the MM-ALE model. The LBE method also required considerably fewer elements in the FE model. Hence, we propose to use the LBE method for simulating blast loads on the bridge decks of long-span steel truss bridges.

Verification of Blast Load Effects on the Steel Members

When a steel truss bridge is subjected to the above-deck close-in explosions, steel truss members of the bridge are indirectly exposed to blast waves rather than the load effects on the bridge deck. The primary target of the simulation of blast loads on the steel truss members is to verify that the simulations could capture the high strain rate effects of steel members observed during the blast tests. Two steel members were numerically analyzed under blast loads by using the LBE method, and the results were compared with the experimental results available in Nassr et al.[20,21]. Two representative blast tests on two steel columns with the section of W150 × 24, nominal length of 2.413 m, and 270 kN of axial load in Nassr et al.[20,21] were considered. In "Blast test I" (blast shot 3), the column was subjected to 150 kg of ANFO at a stand-off distance of 9 m. Similarly, in "Blast test II" (blast shot 1), the mass of the explosive charge and the stand-off distance were set as 50 kg and 10.3 m, respectively. A schematic illustration of the columns with pinned and fixed boundary conditions is shown in Fig. 6. The top end of each member was considered as axially unrestrained, whilst the blast load distribution was uniform along the member. The material model MAT_03 in LS-DYNA was used to simulate the member, and the strain rate effect was considered. The density, yield strength, elastic modulus, and Poisson's ratio of the steel were 7850 kg/m^3, 470 MPa, 210 GPa, and 0.2, respectively. To define the boundary conditions and apply the initial axial loading in the shell and solid finite element models, two rigid plates were used at the top and bottom ends to produce the pinned or fixed conditions, as shown in Fig. 6. Fig. 7 shows the comparison of the mid-span displacement time-histories obtained from the blast tests in Nassr et al.[20,21] and numerical simulations in this study.

As seen in Fig. 7, a close correlation between the simulation results using the LBE method and the test results reported by Nassr et al.[20,21] could be observed. For example, in blast test I, the maximum out-of-plane displacement of the columns obtained from the LBE method using the shell and solid elements were 30.71 and 31.34 mm, respectively. The relative errors of the maximum displacements during the test (31.36 mm for blast test I) with those from simulations using the shell and solid models were 2.07% and 0.01%, respectively. Similarly, for blast test II, the maximum displacements by using the shell and solid models were 5.08 and 5.11 mm, respectively. The corresponding relative errors of the maximum displacement during the test (5.34 mm for blast test II) with those from the shell and solid models were 4.87% and 4.31%, respectively. These relative errors are acceptable, considering the complexity of blast load effects and numerical simulations, and they support the use of the LBE method for investigating the blast load effects on the steel truss members.

Table 2. Comparison of numerical results of the LBE and MM-ALE methods in simulating blast load effects on RC columns

Simulation methods	Peak pressure (MPa)	Maximum disp. (mm)	Blast pressure propagation	Computational time (hours)	Number of elements
LBE	8.1 (8%)	13.9 (11.2%)	No	3.5	68, 260
MM-ALE	7.8 (4%)	12.1 (3.2%)	Yes	33.5	1436, 900

Note: The values in parentheses are the relative errors between the numerical and experimental results.

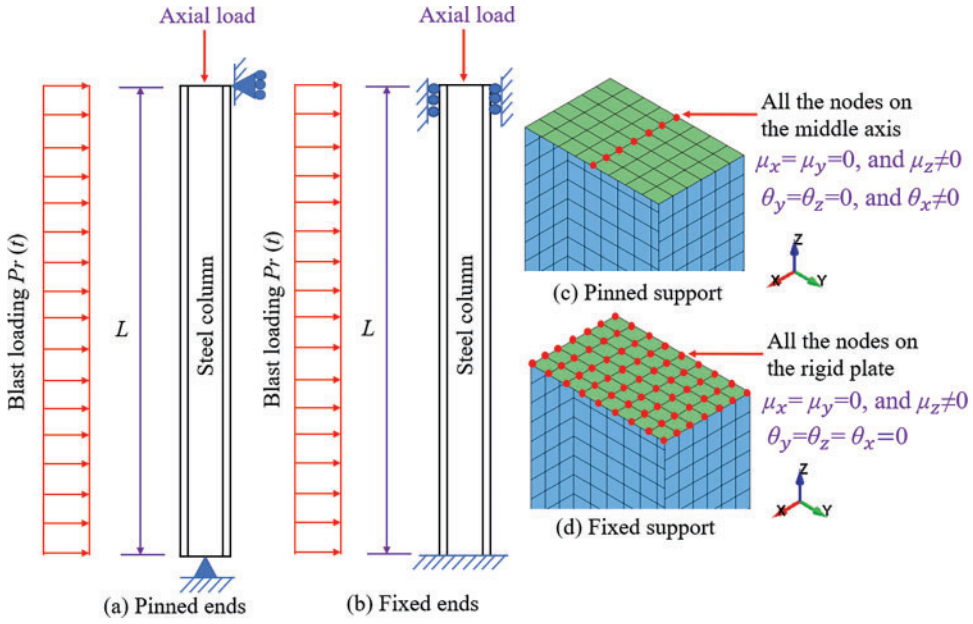

Figure 6. Numerical modeling of the steel columns subjected to the axial load and blast pressure with the pinned and fixed ends

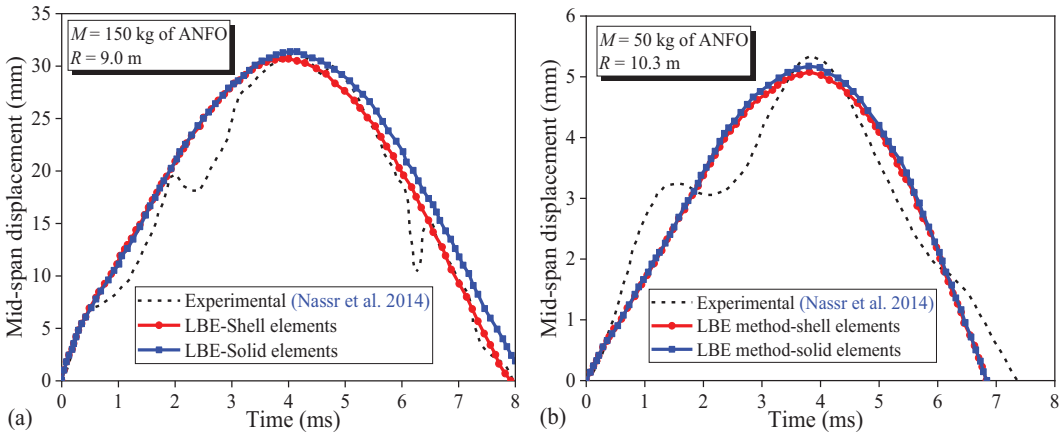

Figure 7. Comparison of the mid-span displacement time-histories of the steel columns from the experimental and numerical results: (a) blast test I and (b) blast test II

Blast Scenarios and Blast Load Cases for the I-35W Steel Truss Bridge

This article defines blast scenarios in terms of vehicle-based terrorist attacks. Similar to several previous studies,[29,51] a virtual scenario describing a terrorist attack carried through explosive-laden vehicles was assumed. According to Thomas et al.,[52] Table 3 presents the impact heights and maximum weight of TNT equivalents carried by several representative vehicle classes without attracting any suspicion. The equivalent TNT mass of up to 1500 kg was considered, which could be classified as a very large load considering the explosive definitions introduced in Lee et al.[51]. Table 4 presents the blast scenarios used to numerically investigate the blast load effects on the I-35W steel truss bridge. Blast load cases (i.e., above-deck close-in explosions) are illustrated in Fig. 2. Two denotation cases in the middle of the center-span were considered, including (i) denotation in the middle of the deck and (ii) denotation on the side of the deck. These two cases are illustrated in Fig. 2 as Case 1 and Case 2, respectively. In the second case of detonation, the side truss of the bridge was directly under the detonation point above the deck.

Blast Load Effects on the Bridge Deck

Concrete can be typically characterized by cracking, crushing, and spalling, whilst reinforcing bars and the steel truss members can be generally characterized by yielding, bulking, and fracture. In this study, the in-elastic response of concrete (i.e., simulated by using the MAT_72R3 material model in LS-DYNA) and steel members (e.g., steel bars and truss members, which were simulated by using the MAT_03 material model in LS-DYNA) could be described by the effective plastic strain and effective plastic strain contours. In order to

Table 3. Impact heights and TNT equivalents of representative vehicle classes

Vehicle	Impact height (m)	Charge capacity (TNT equivalent: kg)
Sedan car	0.61	227
SUV/Van	0.91	454
Small delivery truck	1.22	1814
Water track	1.5	4536
Semi-trailer	1.8	27215

Table 4. Blast scenarios considered for I-35W steel truss bridge

Blast scenario	Vehicle type	TNT explosive mass (kg)	Standoff distance (m)	Scaled distance (m/kg$^{1/3}$)
Scenario A	Sedan car	227	1.0	0.164
Scenario B	SUV/Van	454	1.0	0.130
Scenario C	Truck	1000	1.0	0.1
Scenario D	Truck	1500	1.0	0.087

investigate the possible damage modes and failure characteristics of the bridge, all the above-deck detonations were 1.0 m above the deck vertically. For each denotation case, four blast scenarios, as shown in Table 4, were considered. In these blast scenarios A to D, the mass of the explosives increased from 227 to 1500 kg. Fig. 8 shows the damage modes on the top and bottom faces of the bridge deck for different blast scenarios for blast load case 2 (detonation on the side of the deck), as illustrated in Fig. 2. As seen from Fig. 8, localized damage occurred around the denotation in the bridge deck, and the damage range was found to increase with an increase in the magnitude of the blast load. For example, for blast scenario A (227 kg TNT), a small area of concrete spalled, whereas a crater exceeding 25 square meters was observed for blast scenario D (1500 kg TNT).

Blast Scenarios for the Steel Truss Members: Case 1 (Denotation above the Middle of the Deck)

Fig. 9a shows the damage patterns of steel truss members after blast scenario A for the blast load case 1. It is observed that only several top flanges and webs of the diaphragms yielded and local buckling tended to occur in members. Owing to the strain rate effect of steel, the effective stress of the diaphragm was 586.2 MPa. Hence, the diaphragm was

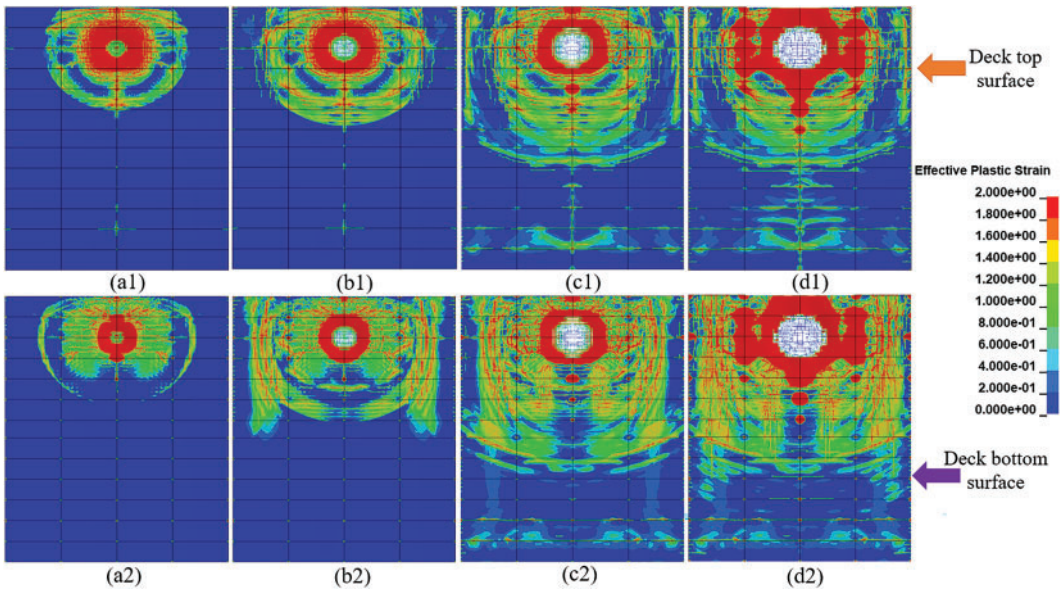

Figure 8. Damage modes of RC deck for denotation above the side of the deck: (a) scenario A, (b) scenario B, (c) scenario C, and (d) scenario D

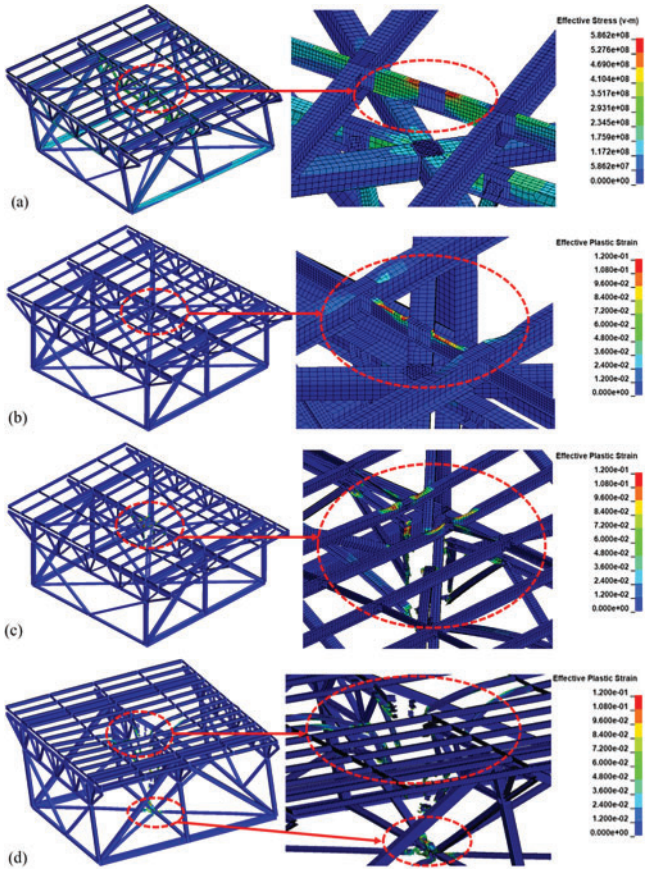

Figure 9. Damage to the steel truss members during different blast scenarios for detonation in the middle of the deck: (a) scenario A, (b) scenario B, (c) scenario C, and (d) scenario D

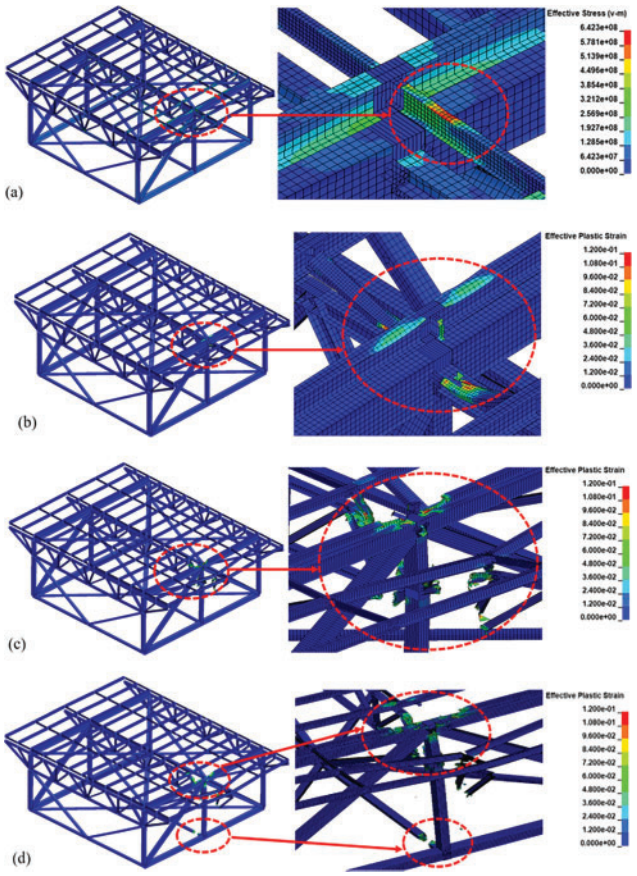

Figure 11. Damage to the steel truss members during different blast scenarios for denotation on the side of the bridge deck: (a) scenario A, (b) scenario B, (c) scenario C, and (d) scenario D

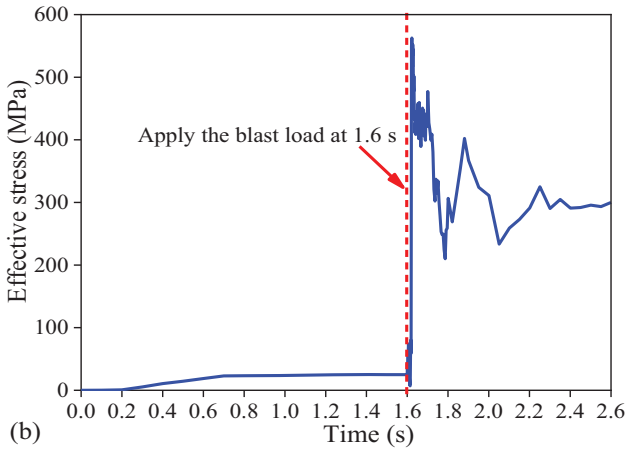

Figure 10. Effective stress time-history of the steel truss members for blast scenario B for denotation above the middle of the deck (blast load case 1)

plastically deformed but not fractured. With an increase in the magnitude of blast load in scenarios B, C and D, the severity of the damage in the truss members increased, as shown in Figs. 9b–9d. In addition to the increased damage severity to the secondary members, such as diaphragms, the primary loading-carrying members on the side trusses (i.e., diagonal members, upper chords, and lower chords) remained elastic for scenario B, upper braces and floor truss members were damaged during scenario C, and many lower floor truss members and lower braces were damaged during scenario D. Even under blast scenario D, damages to the primary loading-carrying members on the side trusses was still relatively less severe. However, severe damage to several secondary truss members, particularly in scenario D, may increase the risk of progressive collapse of the bridge because of their critical role in maintaining the stability of the truss bridge. The dynamic response of the truss elements during the blast load is shown in Fig. 10 for blast load scenario B, which shows the effective stress time history of the shell element that was located at one of the yielded stringers. It is observed that the target shell element underwent dynamic vibration with a peak dynamic amplitude of 560 MPa (which was only 40 MPa under the service load condition: dead load (DL) + live load (LL) case). After this vibration was damped out, the bridge reached a new steady state with an effective stress of 300 MPa in the target shell element, indicating substantial permanent damage to the affected truss members. Similar behavior was observed during other blast load scenarios, although with different levels of severity, depending on the blast intensity.

Blast Scenarios for the Steel Truss Members: Case 2 (Denotation above the Side of the Deck)

Fig. 11a shows the damage modes of truss members after blast scenario A for denotation above the side bridge deck. Simulation results showed that only one transverse diaphragm yielded. The effective stress in this diaphragm was 642.3 MPa. Thus, the diaphragm was plastically deformed but not fractured. The severity of damage in the bridge increased with an increase in the blast intensity, as shown in Figs. 11b–11d for blast scenarios B to D, respectively. For instance, in blast scenario B, several transverse diaphragms buckled and fractured, and some of the top flanges of stringers yielded and exhibited plastic deformations. However, damage to the bridge was localized and truss members on the side trusses were still in the elastic range. Under blast scenario C, additional lateral buckling of many stringers, fracture of several transverse diaphragms and floor truss members, and damage to the side truss members, such as yielding of the top flanges of upper chords and webs of the vertical members located directly under the explosive charge, were also observed. For blast scenario D, besides the increase in the severity of damage to truss members under scenario C, one of the lower bottom crossbeams was damaged. With damage propagating to the primary load-carrying truss members in the side truss, this blast scenario represents a critical case for the truss bridge.

UHPC Strengthening of the Deck

Results presented above show that the damage to the steel truss members propagated following the damage to the deck. Hence, improvement in the blast resistance of the deck could be effective in reducing damage propagated to the steel truss members below. A recent study by Su et al.[35] has shown that decks made of ultra-high-performance concrete UHPC generally have better blast resistance than those made from normal strength concrete (NSC). Hence, further simulations have been carried out by replacing the bridge deck with that made from UHPC. Simulation of the UHPC deck in LS-DYNA has been done by considering the material model MAT_72R3 with the material parameters calibrated by Su et al.[35] based on the experimental results.

According to Su et al.,[35] the UHPC slabs were prefabricated by mixing the Chinese standard Graded 52.5 P.II type Portland cement, silica fume, ultra-fine mineral admixture which consists of fly ash and ultra-fine slag, the natural river sand with a maximal diameter of 2.5 mm, polycarboxylic type high-range-water-reducer (HRWR) and 2% (volume fraction) straight brass-coated steel fiber. The mixture proportions of the UHPC material are given in Table 5. Based on Chinese specification GB-T50081-2002, the compressive strength and splitting tensile strength of the NSC specimens are 30.4 MPa and 3.36 MPa, respectively. Correspondingly, the compressive strength and the direct tensile strength of the UHPC specimens are 125.27 MPa and 8.33 MPa, respectively. In addition, Fig. 12 shows a comparison between the post-blast damage modes of a UHPC bridge deck based on experimental and simulation results. This figure shows that the simulation results agreed well with those from the

Table 5. Mixture proportions of the UHPC material (kg/m^3)

Cement	Silica fume	Ultra-fine mineral admixture	Sand	Water	HRWR	Steel fibers
700	140	110	1200	152	22.8	145

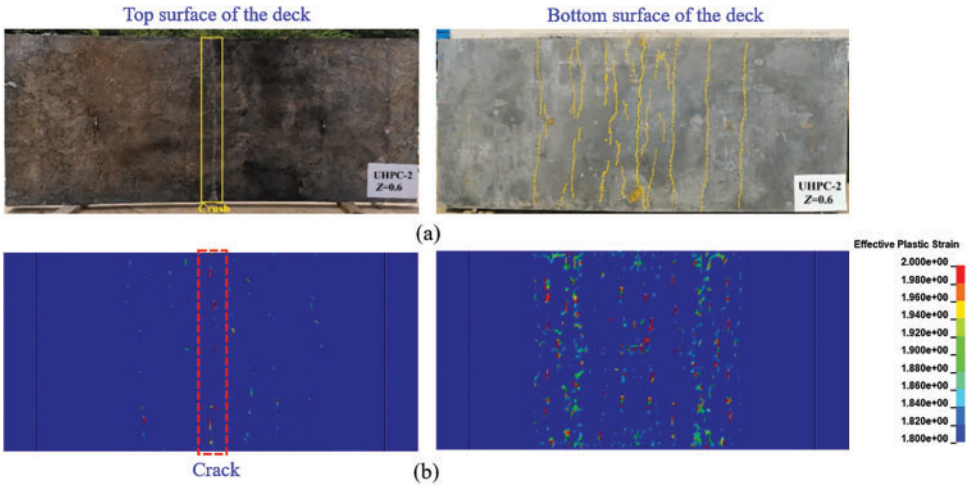

Figure 12. Comparison of the experimental and numerical post-blast damage modes for UHPC deck under the blast intensity of $Z = 0.6$ m/kg$^{1/3}$: (a) test results in Su et al.[35] and (b) numerical results in this study

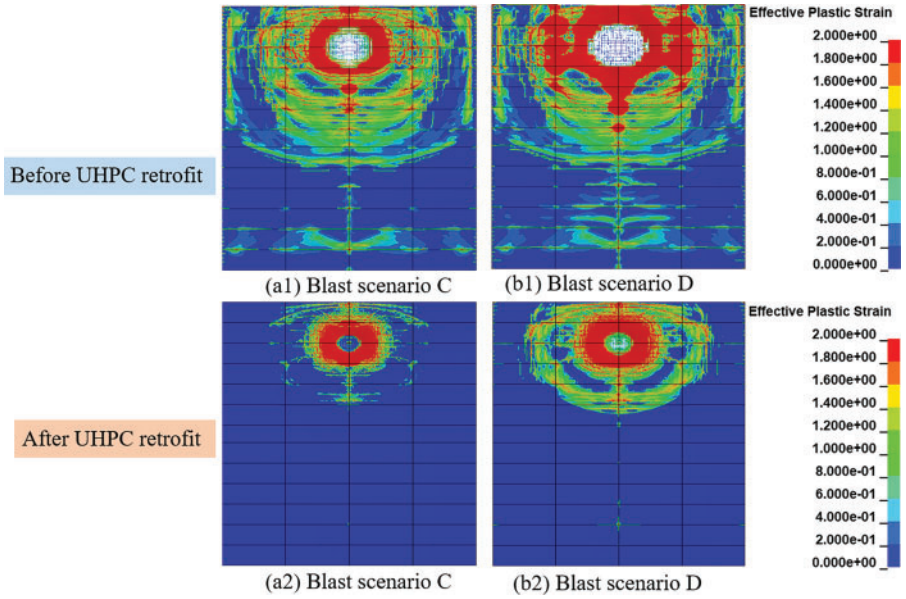

Figure 13. Damage modes of the deck (top surface) before and after UHPC strengthening for denotation above the side bridge deck of the bridge

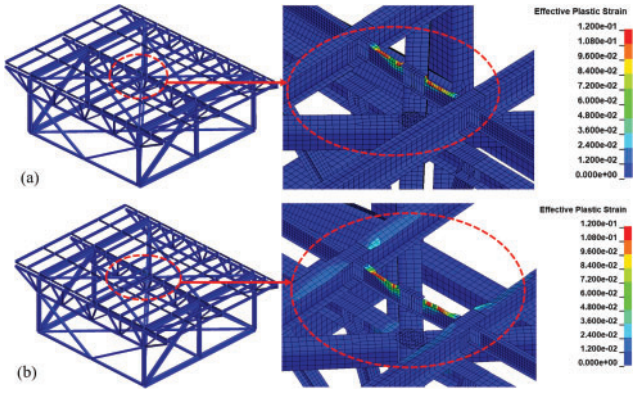

Figure 14. Damage to the steel truss members under different blast scenarios for denotation on the middle of the bridge deck: (a) scenario C and (b) scenario D

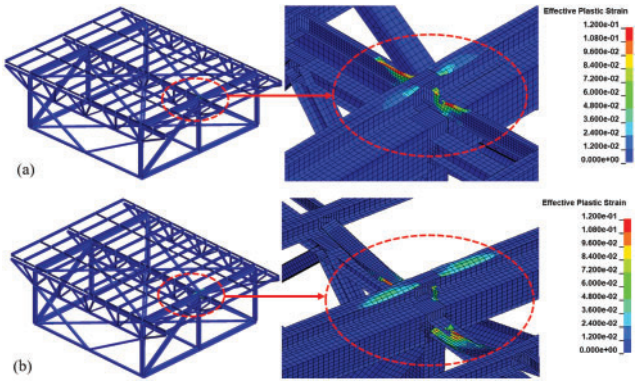

Figure 15. Damage to the steel truss members under different blast scenarios for denotation on the side of the bridge deck: (a) scenario C and (b) scenario D

test. Thus, simulations on blast load effects on the bridge with UHPC deck were carried out to investigate damage to steel truss members under different blast load scenarios investigated previously.

Fig. 13 shows a comparison of the damage modes of the deck with and without UHPC strengthening for blast scenarios C and D when the detonation was near the side of the bridge deck. It is observed that although similar localized damages in the bridge deck were observed around the denotation, the damaged area was reduced significantly in the case of the UHPC deck. For instance, for blast scenario D, the NSC deck had a crater with an area of over 25 square meters. This area was reduced to 5 square meters for the UHPC deck. With an almost 80% reduction in the size of the crater, the blast load effect transmitted to steel truss members below would also be reduced proportionately. Hence, UHPC could be used to reduce the risk of severe damage to the bridge decks vulnerable to blast loads.

Fig. 14 shows the damage modes of the truss members for the bridge with the UHPC deck for blast scenarios C and D for the blast load case 1. Comparing results in Fig. 14a to those in Fig. 9c for the NSC deck for blast scenario C indicates that the damage to the truss bridge was limited to buckling and fracture of several transverse diaphragms in the case of the UHPC deck, whereas severe damage to several stringers, transverse diaphragms, upper braces, and floor truss members occurred in the case of the NSC deck. Likewise, as seen from Fig. 14b, for blast scenario D, the only additional damage with respect to scenario C in the case of the UHPC deck was plastic deformation and yielding on the top flanges of stringers, and the bridge was not vulnerable to the risk of progressive collapse. Results for the blast load Case 2 are shown in Fig. 15 for blast scenarios C and D, respectively. These results are similar to those for the blast load case 1 and indicate that the UHPC deck was able to

prevent any significant damage to the primary load-carrying truss members on the side truss.

Conclusions

This article presents the results of a comprehensive numerical investigation of the damage modes and damage mechanism of long-span steel truss bridges subjected to the above-deck explosions. The I-35W truss bridge in Minneapolis, MN, that collapsed in 2008 was used as a case study because of the availability of detailed information on the bridge drawings and several investigations following the collapse of the bridge. Various blast scenarios based on common vehicle-based explosions with explosives weight up to 1500 kg equivalent of TNT placed 1 m above the bridge deck were considered. Numerical simulations were carried out to evaluate both the Load_Blast_Enhanced (LBE) function and Multi-Material Arbitrary Lagrangian-Eulerian (MM-ALE) method in LS-DYNA for applying blast loads to the bridge deck. Simulation results showed that the LBE function in LS-DYNA was reasonably accurate and computationally cost-effective, as well as conservative, and it could be used to apply blast load effects on the case-study bridge. Since the blast load effects depend on the material models because of strain rate effects, the simulation of blast loads on both the concrete bridge deck and steel members were compared with the blast test results available in the literature in order to ensure the reliability and accuracy of the numerical results.

In addition, two cases of blast loads (above the middle and side of the deck) and four blast scenarios in terms of the weight of the explosives, damage modes of the deck, and steel truss members were examined in detail. Simulation results show that both the damage range and area of the deck and steel truss members tended to increase with the increase in blast intensity. Based on this, the finite element model of the bridge had a blast zone where detailed modeling using both the beam and shell elements (i.e., multi-scale modeling technique) was done. A portion of the bridge outside the blast zone was modeled only by beam elements. The size of elements within the blast zone was also much smaller than those outside the blast zone. This was done to ensure accuracy while managing the computational time to the feasible level.

For the concrete deck, it was observed that the size of the crater in the deck increased from blast scenarios A to D and was approximately 25 square meters for scenario D for 1500-kg TNT weight. For the steel truss members, the damage mode of the truss bridge changed from several transverse diaphragms plastically deformed or laterally buckled only to some of the primary load-carrying truss members on the side truss damaged as the blast intensity increased from blast scenario A (275-kg TNT) to blast scenario D (1500-kg TNT). In addition, damage to the truss bridge system was also propagated from the upper to the lower truss system with the increase in blast loads. Most significant risk of progressive collapse of the bridge came from damage to several secondary members, such as the steel diaphragms, stringers, floor truss members, and braces, which are critical in ensuring the stability of the truss bridge. The feasibility of using UHPC to improve the blast resistance of the truss bridge was studied. Simulation results show that the size of the crater in the UHPC deck decreased by almost 80% during blast scenario D with respect to that for the NSC. Blast load effects on the steel truss members also decreased significantly when a UHPC deck was used.

Simulation results presented in this article are based on the use of the LBE function in LS-DYNA to impose blast load effects on the bridge. This simplification ignores reflections of blast load that may occur because of the bridge geometry (e.g., an explosion in a closed geometry). For such situations, the use of the MM-ALE method may be more appropriate. However, it is significantly more computationally expensive because of modeling on air around the bridge in the blast zone.

Acknowledgments

This material is based upon work supported by the Federal Highway Administration under contract number DTFH61-14-D-00010/0004 and the City University of New York High-Performance Computing Center at the College of Staten Island. Any opinions, findings, and conclusions or recommendations expressed in this publication are those of the authors and do not necessarily reflect the views of the Federal Highway Administration.

Data Availability Statement

All the data, models, or codes that support the findings of this study are available from the corresponding author upon reasonable request.

References

[1] Draganić H, Gazić G, Varevac D. Experimental investigation of design and retrofit methods for blast load mitigation-A state-of-the-art review. *Eng Struct*. 2019;190:189–209. doi:10.1016/j.engstruct.2019.03.088.

[2] Li HH. *Alternate Load Paths and Retrofits for Long-Span Truss Bridges Under Sudden Member Loss and Blast Loads*. Ph.D. Thesis. Dept. of Civil Engineering, The City University of New York, New York, NY, USA; 2021.

[3] Yi Z, Agrawal AK, Ettouney M, et al. Blast load effects on highway bridges. I: modeling and blast load effects. *ASCE J Bridge Eng*. 2014;19(4):04013023. doi:10.1061/(ASCE)BE.1943-5592.0000547.

[4] Yi Z, Agrawal AK, Ettouney M, et al. Blast load effects on highway bridges. II: failure modes and multihazard correlations. *ASCE J Bridge Eng*. 2014;19(4):04013024. doi:10.1061/(ASCE)BE.1943-5592.0000548.

[5] Duwadi SR, Chase SB. Multiyear plan for bridge and tunnel security research, development, and deployment. Report No: FHWA-HRT-06-072. Springfield, VA: FHWA; 2006.

[6] Zhang C, Gholipour G, Mousavi AA. Blast loads induced responses of RC structural members: state-of-the-art review.

Compos Part B: Eng. 2020;195(1):108066. doi:10.1016/j.compositesb.2020.108066.

[7] U.S. Department of Defense (USDOD). *Structures to Resist the Effects of Accidental Explosions*. Washington, DC: UFC 3-340-02; 2008.

[8] El-Dakhakhni WW, Mekky WF, Changiz-Rezaei SH. Vulnerability screening and capacity assessment of reinforced concrete columns subjected to blast. *ASCE J Perform Construct Facil*. 2009;23(5):353–365. doi:10.1061/(ASCE)CF.1943-5509.0000015.

[9] AUTODYN. *Interactive Non-Linear Dynamic Analysis Software, Version 12, User's Manual*. Canonsburg, PA: SAS IP Inc; 2009.

[10] ABAQUS. *Analysis User's Manual Version 6.10*. Volume I to VI. Providence, RI: ABAQUS; 2010.

[11] LSTC (Livermore Software Technology Corporation). LS-DYNA® keywords user manual Volume II-Material models. 2020. Accessed September 9, 2020. https://www.dynasupport.com/manuals/ls-dyna-manuals/ls-dyna_manual_volume_i_r12.pdf.

[12] Shin J, Jeon JS. Retrofit scheme of FRP jacketing system for blast damage mitigation of non-ductile RC building frames. *Compos Struct*. 2019;228(5):111328. doi:10.1016/j.compstruct.2019.111328.

[13] Gomathi KA, Rajagopal A, Reddy KSS, et al. Plasticity based material model for concrete subjected to dynamic loadings. *Int J Impact Eng*. 2020;142(1):103581. doi:10.1016/j.ijimpeng.2020.103581.

[14] Castedo R, Santos AP, Alañón A, et al. Numerical study and experimental tests on full-scale RC slabs under close-in explosions. *Eng Struct*. 2021;231:111774. doi:10.1016/j.engstruct.2020.111774.

[15] Xiao W, Andrae M, Gebbeken N. Numerical study of blast mitigation effect of innovative barriers using woven wire mesh. *Eng Struct*. 2020;213(6):110574. doi:10.1016/j.engstruct.2020.110574.

[16] Williamson EB, Bayrak O, Davis C, et al. Performance of bridge columns subjected to blast loads. I: experimental program. *ASCE J Bridge Eng*. 2011;16(6):693–702. doi:10.1061/(ASCE)BE.1943-5592.0000220.

[17] Williamson EB, Bayrak O, Davis C, et al. Performance of bridge columns subjected to blast loads. II: results and recommendations. *ASCE J Bridge Eng*. 2011;16(6):703–710. doi:10.1061/(ASCE)BE.1943-5592.0000221.

[18] Foglar M, Hajek R, Fladr J, et al. Full-scale experimental testing of the blast resistance of HPFRC and UHPFRC bridge decks. *Construct Build Mater*. 2017;145(5):588–601. doi:10.1016/j.conbuildmat.2017.04.054.

[19] Nagata M, Beppu M, Ichino H, et al. A fundamental investigation of reinforced concrete beams subjected to close-in explosion. *Int J Protect Struct*. 2018;9(2):174–198. doi:10.1177/2041419617716483.

[20] Nassr AA, Razaqpur AG, Tait MJ, et al. Strength and stability of steel beam columns under blast load. *Int J Impact Eng*. 2013;55(4):34–48. doi:10.1016/j.ijimpeng.2012.11.010.

[21] Nassr AA, Razaqpur AG, Tait MJ, et al. Dynamic response of steel columns subjected to blast loading. *ASCE J Struct Eng*. 2014;140(7):04014036. doi:10.1061/(ASCE)ST.1943-541X.0000920.

[22] Mazurkiewicz L, Malachowski J, Baranowski P. Blast loading influence on load carrying capacity of I-column. *Eng Struct*. 2015;104(10):107–115. doi:10.1016/j.engstruct.2015.09.025.

[23] Al-Thairy H. A modified single degree of freedom method for the analysis of building steel columns subjected to explosion induced blast load. *Int J Impact Eng*. 2016;94(3):120–133. doi:10.1016/j.ijimpeng.2016.04.007.

[24] Momeni M, Hadianfard MA, Bedon C, et al. Numerical damage evaluation assessment of blast loaded steel columns with similar section properties. *Structures*. 2019;20(4):189–203. doi:10.1016/j.istruc.2019.04.002.

[25] Hao H, Tang EK. Numerical simulation of a cable-stayed bridge response to blast loads, Part II: damage prediction and FRP strengthening. *Eng Struct*. 2010;32(10):3193–3205. doi:10.1016/j.engstruct.2010.06.006.

[26] Williams GD, Williamson EB. Response of reinforced concrete bridge columns subjected to blast loads. *ASCE J Struct Eng*. 2011;137(9):903–913. doi:10.1061/(ASCE)ST.1943-541X.0000440.

[27] Pan Y, Chan BY, Cheung MM. Blast loading effects on an RC slab-on-girder bridge superstructure using the multi-Euler domain method. *ASCE J Bridge Eng*. 2013;18(11):1152–1163. doi:10.1061/(ASCE)BE.1943-5592.0000457.

[28] Pan Y, Ventura CE, Cheung MM. Performance of highway bridges subjected to blast loads. *Eng Struct*. 2017;151(10):788–801. doi:10.1016/j.engstruct.2017.08.028.

[29] Zhu Z, Li Y, Ma C. Damage analysis of small box girder bridges under car explosion. *Eng Fail Anal*. 2021;120(6):105104. doi:10.1016/j.engfailanal.2020.105104.

[30] Abada M, Ibrahim A. Hybrid multi-cell thin-walled tubes for energy absorption applications: blast shielding and crashworthiness. *Compos Part B: Eng*. 2020;183(9):107720. doi:10.1016/j.compositesb.2019.107720.

[31] Liu L, Zong Z, Gao C, et al. Experimental and numerical study of CFRP protective RC piers under contact explosion. *Comp Struct*. 2020;234(6):111658. doi:10.1016/j.compstruct.2019.111658.

[32] Jacques E, Lloyd A, Imbeau P, et al. GFRP-retrofitted reinforced concrete columns subjected to simulated blast loading. *ASCE J Struct Eng*. 2015;141(11):04015028. doi:10.1061/(ASCE)ST.1943-541X.0001251.

[33] Li J, Wu C, Hao H, et al. Experimental and numerical study on steel wire mesh reinforced concrete slab under contact explosion. *Mater Des*. 2017;116:77–91. doi:10.1016/j.matdes.2016.11.098.

[34] Li J, Wu C. Damage evaluation of ultra-high performance concrete columns after blast loads. *Int J Protect Struct*. 2018;9(1):44–64. doi:10.1177/2041419617743986.

[35] Su Q, Wu H, Sun HS, et al. Experimental and numerical studies on dynamic behavior of reinforced UHPC panel under medium-range explosions. *Int J Impact Eng*. 2021;148(10):103761. doi:10.1016/j.ijimpeng.2020.103761.

[36] Astarlioglu S, Krauthammer T. Response of normal-strength and ultra-high-performance fiber-reinforced concrete columns to idealized blast loads. *Eng Struct*. 2014;61:1–12. doi:10.1016/j.engstruct.2014.01.015.

[37] Aoude H, Dagenais FP, Burrell RP, et al. Behavior of ultra-high-performance fiber reinforced concrete columns under blast loading. *Int J Impact Eng*. 2015;80(5):185–202. doi:10.1016/j.ijimpeng.2015.02.006.

[38] Astaneh-Asl A. Progressive collapse of steel truss bridges, the case of I-35W collapse. *Proceedings of 7th International Conference on Steel Bridges*; 2008; Guimarães, Portugal.

[39] Ocel JM, Wright WJ. *Finite Element Modeling of I-35W Bridge Collapse-Final Report*. Washington, DC: Federal Highway Administration, Turner-Fairbank Highway Research Center; 2008.

[40] Hao S. I-35W bridge collapse. *J Bridge Eng*. 2010;15(5):608–614. doi:10.1061/(ASCE)BE.1943-5592.0000090.

[41] Liao M, Okazaki T, Ballarini R, et al. Nonlinear finite-element analysis of critical gusset plates in the I-35W bridge in Minnesota. *ASCE J Struct Eng*. 2011;137(1):59–68. doi:10.1061/(ASCE)ST.1943-541X.0000269.
[42] Higgins C, Dusicka P, Scott M. Experimental tests and numerical analyses of steel truss bridge gusset connections. Rep. No. OTREC-RR-12-03. Portland, OR: OTREC; 2012.
[43] Agrawal AK, Mohammed E, Chen X, et al. Steel truss retrofits to provide alternate load paths for cut or blast-damaged or destroyed members. Rep. No. FHWA-HRT-20-055. McLean, VA: Federal Highway Administration; 2020.
[44] Li HH, Agrawal AK, Chen X, et al. A framework for identification of the critical members for truss bridges through nonlinear dynamic analysis. *ASCE J Bridge Eng*. 2022; 27(8):04022060. doi:10.1061/(ASCE)BE.1943-5592.0001902.
[45] Li HH, Zhou GJ, Wang J. A generalized framework for the alternate load path redundancy analysis of steel truss bridges subjected to sudden member loss scenarios. *Buildings*. 2022;12(10):1597. doi:10.3390/buildings12101597.
[46] Chen X, Li HH, Agrawal AK, et al. Alternate load paths redundancy analysis of steel truss bridges. *ASCE J Bridge Eng*. 2022;27(11):04022106. doi:10.1061/(ASCE) BE.1943-5592.0001943.
[47] Chen X, Li HH, Agrawal AK, et al. Performance-based retrofits of long-span truss bridges based on the alternate load path redundancy analysis. *J Bridge Eng*. 2023;28(2):04022141. doi:10.1061/JBENF2.BEENG-5354.
[48] Wang W, Zhang D, Lu F, et al. Experimental study and numerical simulation of the damage mode of a square reinforced concrete slab under close-in explosion. *Eng Fail Anal*. 2013;27(1):41–51. doi:10.1016/j.engfailanal.2012.07.010.
[49] Tang EK, Hao H. Numerical simulation of a cable-stayed bridge response to blast loads, Part I: model development and response calculations. *Eng Struct*. 2010;32(10):3180–3192. doi:10.1016/j.engstruct.2010.06.007.
[50] Li J, Hao H. Numerical study of concrete spall damage to blast loads. *Int J Impact Eng*. 2014;68:41–55. doi:10.1016/ j.ijimpeng.2014.02.001.
[51] Lee J, Choi K, Chung C. Numerical analysis-based blast resistance performance assessment of cable-stayed bridge components subjected to blast loads. *Appl Sci*. 2020;10(23): 8511. doi:10.3390/app10238511.
[52] Thomas RJ, Steel K, Sorensen AD. Reliability analysis of circular reinforced concrete columns subject to sequential vehicular impact and blast loading. *Eng Struct*. 2018; 168(3):838–851. doi:10.1016/j.engstruct.2018.04.099.